Eur. J. Mineral., 36, 899–916, 2024
https://doi.org/10.5194/ejm-36-899-2024

European Journal of Mineralogy
Open Access

Experimental petrology constraints on kamafugitic magmas

Francesca Innocenzi[1,2,3], **Isra S. Ezad**[3,4], **Sara Ronca**[1], **Samuele Agostini**[2], **Michele Lustrino**[1,5], **and Stephen F. Foley**[3,6]

[1]Dipartimento di Scienze della Terra, Sapienza Università di Roma, Rome, 00185, Italy
[2]Istituto di Geoscienze e Georisorse – CNR, Pisa, 56124, Italy
[3]School of Natural Sciences, Macquarie University, North Ryde, New South Wales 2109, Australia
[4]Centre for Exploration Targeting, School of Earth Sciences, University of Western Australia, Perth, Western Australia 6009, Australia
[5]Istituto di Geologia Ambientale e Geoingegneria – CNR, c/o Dipartimento di Scienze della Terra, Sapienza Università di Roma, Rome, 00185, Italy
[6]Research School of Earth Sciences, Australian National University, Canberra, Australian Capital Territory 2600, Australia

Correspondence: Francesca Innocenzi (francesca.innocenzi@uniroma1.it)

Received: 14 February 2024 – Revised: 12 August 2024 – Accepted: 16 August 2024 – Published: 9 October 2024

Abstract. Kamafugites are rare volcanic igneous rocks, characterized by the presence of kalsilite and variable amounts of leucite, nepheline, melilite, clinopyroxene, olivine and phlogopite, which may not necessarily be present all together. Kamafugites are silica-poor (moderately ultrabasic to basic), CaO- and alkali-rich (mostly ultrapotassic) lithologies, generated from strongly metasomatized and heterogeneous mantle sources, with abundant phlogopite and little or no orthopyroxene. Melting of phlogopite- and carbonate-bearing veins is often invoked as being responsible for the ultrapotassic and ultracalcic signatures observed in many kamafugites. Nevertheless, many questions still persist about their mantle sources, such as the paragenesis of the metasomatic veins within the lithospheric mantle and the degree of interaction between the initial melts and the peridotite matrix.

We experimentally investigated four natural kamafugite samples to determine the mantle assemblages that were in equilibrium with these melts at the onset of partial melting and their genesis. The kamafugites were collected from the three known areas where they occur: Uganda, Italy and Brazil. Near-liquidus experiments were carried out at 1 to 2 GPa and temperatures from 1250 to 1380 °C. These experiments provide information on the mineralogy of the potential mantle sources in each of the volcanic provinces, also allowing a comparison among them. The experiments confirm the common presence of clinopyroxene and phlogopite as the main near-liquidus phases, with olivine joining the near-liquidus phase assemblage in one Italian sample (San Venanzo) and in the Brazilian kamafugite. Other minor phases (apatite and Fe–Ti oxides) also crystallized in near-liquidus conditions, highlighting their importance for at least the Ugandan and Brazilian kamafugites. Our results demonstrate that various amounts of clinopyroxene (∼ 40 % in Italy and 50 %–60 % in Uganda and Brazil), phlogopite (∼ 20 %–30 % in Brazil, ∼ 40 % in Uganda and ∼ 60 % in Italy) and accessory phases (up to 4 % titanite in Uganda, up to 3 % apatite in Uganda and up to 5 % oxides in Uganda and Brazil) are required for the formation of kamafugite melts. The contribution of olivine differs among the four samples, being negligible for the Ugandan kamafugites and in one of the Italian kamafugites but up to 5 % in the second Italian kamafugite and 10 % in Brazil.

1 Introduction

The Earth's mantle is heterogeneous in terms of mineralogy, chemistry and isotopic compositions, mostly due to long-lasting cycles of recycling in convergent zones, magma extraction and upwelling (Anderson, 2006; Stixrude and Lithgow-Bertelloni, 2012). Consequently, partial melting events in the upper mantle potentially involve depleted and variably enriched mantle components, including recycled crustal lithologies and the interaction products between melts derived therefrom and the peridotitic matrix, causing compositional variability in the resulting igneous products (e.g. Stracke, 2021). Partial melting of a metasomatized lithosphere consisting of two or more distinct rock types is often invoked for exotic and volatile-rich alkaline magmas, such as kamafugites (Foley, 1992a; Prelević et al., 2013).

The ultimate composition of kamafugite mantle sources and their degree of partial melting are still under debate. Recycling of crustal materials into the lithospheric mantle could stabilize K-rich phases such as phlogopite, also allowing for the development of carbonate phases and melts with carbonatite compositions. H_2O–CO_2-bearing pyroxenites, together with carbonate melts, are often assumed to be fundamental components in the formation of low-silica ultrapotassic melts (e.g. Foley et al., 2002; Tappe et al., 2008; Gülmez et al., 2023). Ultramafic nodules found in kamafugite lavas support the idea of a metasomatized mantle. They are particularly common in Uganda, where they show a phlogopite-bearing clinopyroxenite to clinopyroxene-bearing glimmerite composition (i.e. rocks made totally – or almost totally – of brown mica; Le Maitre, 2002), with accessory magnetite, titanite, apatite, perovskite and Ca-carbonate (Link et al., 2008; Pitcavage et al., 2021; Innocenzi et al., 2022, 2024a). No garnet or orthopyroxene is found in the Ugandan nodules, whilst olivine is extremely rare (Link et al., 2008). Nodules in Brazilian kamafugites are garnet lherzolites to spinel lherzolites and glimmerites, as well as metasomatized peridotites with enrichments in phlogopite, ilmenite and chromite (Carvalho and Leonardos, 1995; Gaspar et al., 2003). No ultramafic nodules are currently known in the Italian kamafugites (e.g. Lustrino et al., 2020).

Melting experiments play a key role in constraining the mineralogy of the mantle source, solidus temperatures and mechanisms leading to the formation of primitive melts. Some of these melting experiments have focused on the melting of a modified peridotite (Foley and Pintér, 2018) by adding $H_2O \pm CO_2$ (e.g. Wallace and Green, 1988; Pintér et al., 2021), or pyroxenite and eclogite ($\pm$ amphibole and phlogopite) compositions (e.g. Pertermann and Hirschmann, 2003; Förster et al., 2019; Foley et al., 2022; Foley and Ezad, 2024). More recent reaction experiments have used mixed sediments and synthetic or natural upper-mantle compositions (e.g. Gülmez et al., 2023). Unfortunately, only a smaller number of experiments, including both melting experiments (e.g. Foley et al., 2022; Lloyd et al., 1985; Funk and Luth, 2013) and liquidus surveys (e.g. Edgar et al., 1976), have focused on the mantle sources of primitive ultrapotassic melts and even fewer have investigated liquidus phase compositions of natural kamafugitic melts.

Nearly all of the few experiments conducted on kamafugitic melts have focused on the Ugandan ultrapotassic suite (e.g. Lloyd, 1985; Lloyd et al., 1985; Edgar et al., 1976) due to their abundance of ultramafic xenoliths, interpreted to be either the magma source or cumulates from kamafugitic melts (e.g. Lloyd, 1981; Link et al., 2010; Muravyeva and Senin, 2018), along with good preservation of the lava flows. The scarcity of experimental constraints, together with the ambiguous experimental results, is the backdrop to our experimental investigation focusing specifically on kamafugitic magmas. By conducting near-liquidus experiments at 1–2 GPa and 1250–1380 °C on natural kamafugite samples, this experimental study aims to constrain the mineral phases in equilibrium with kamafugite liquids and to reconstruct the likely source mineralogy and the modal percentage of phases entering the melt.

2 Starting materials

Kamafugites are kalsilite-bearing volcanic rocks (Le Maitre, 2002), a very rare group of ultrapotassic lithologies with K_2O and MgO > 3 wt % and $K_2O / Na_2O > 2$ (Foley et al., 1987; Lustrino et al., 2020; Oliveira et al., 2022). They have low silica (< 46 wt %), low Al_2O_3 and Na_2O, and high CaO contents (Foley et al., 1987). They are feldspar-free rocks, with variable amounts of olivine, clinopyroxene, phlogopite, leucite, melilite, perovskite and carbonate and the fundamental presence of kalsilite (Foley et al., 1987; Le Maitre, 2002; Tappe et al., 2003; Oliveira et al., 2022).

Typical kamafugite rocks (i.e. with primary kalsilite) are found in three regions only:

1. The first region comprises the Middle Pleistocene ($\sim$ 188 ka; Rosenthal et al., 2009) Toro Ankole volcanic district (TA; Fig. 1a; Holmes, 1950) in the western branch of the East African Rift, associated with carbonatites, foidites and melilitites (Holmes, 1952; Rosenthal et al., 2009; Muravyeva et al., 2014; Innocenzi et al., 2024a).

2. The second region comprises the Middle Pleistocene San Venanzo (SAV) and Cupaello (CUP) volcanoes in central Italy (Fig. 1b), which belong to the Intra-Apennine Province (IAP; Gallo et al., 1984; Stoppa and Cundari, 1998; Lustrino et al., 2020). A recent study also revealed the presence of kalsilite in melilite-bearing lavas from a neighbouring district (Pleistocene Montefiascone Volcanic Complex – Vulsini Mountains), belonging to the Roman Comagmatic Region (Innocenzi et al., 2024b).

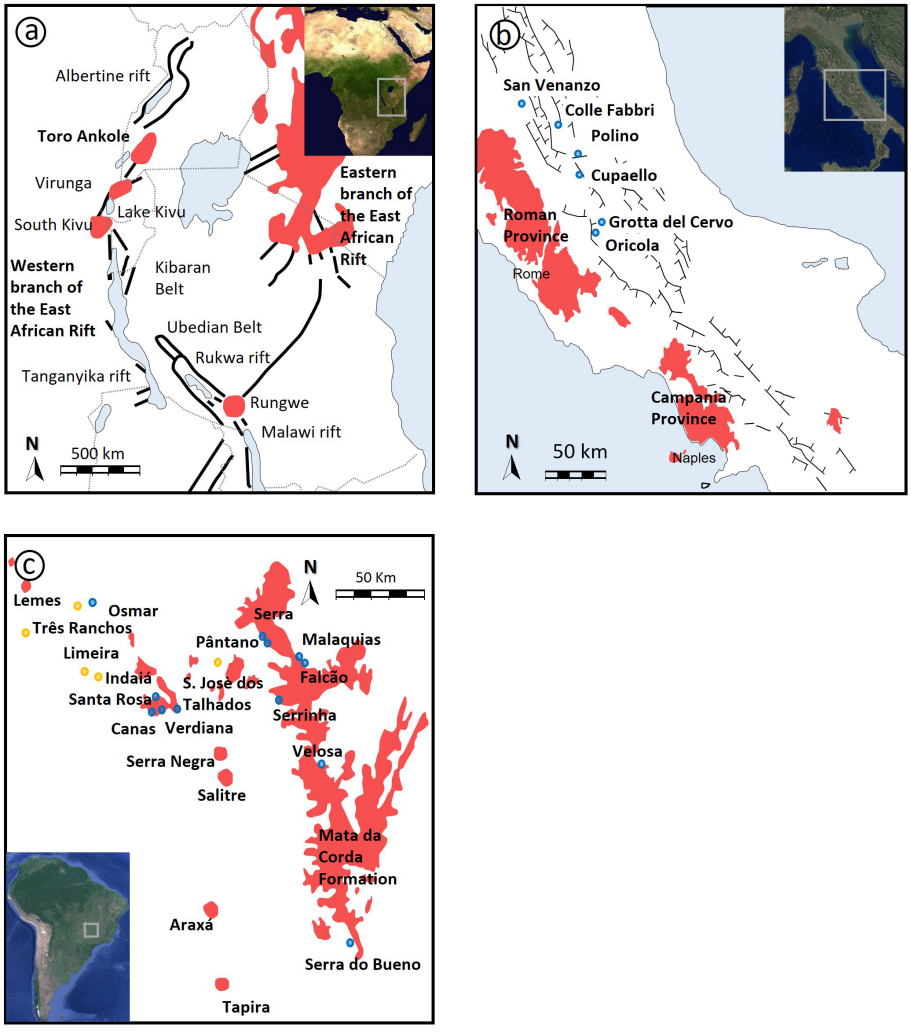

Figure 1. **(a)** Geological sketch of eastern Africa showing the location of the Toro Ankole Volcanic Province along the western branch of the East African Rift. In red are volcanics in the eastern and the western branches of the East African Rift. Toro Ankole, Virunga, South Kivu and Rungwe are the four volcanic provinces of the western branch. Black denotes main faults. Modified after Innocenzi et al. (2024a). **(b)** Geological sketch of the Intra-Apennine Province. Blue denotes eruptive centres (San Venanzo, Colle Fabbri, Polino, Cupaello, Grotta del Cervo and Oricola), and red denotes principal volcanic provinces in central Italy (Roman Province, Ernici–Roccamonfina and Campania provinces, and the Monte Vulture volcano). Modified after Lustrino et al. (2020). **(c)** Geological sketch of the Alto Paranaíba Igneous Province. Red denotes the Mata Da Corda Formation, blue denotes kamafugite outcrops, and yellow denotes kimberlite outcrops. Modified after Melluso et al. (2008) and Guarino et al. (2013).

3. The third region comprises the Late Cretaceous Alto Paranaíba Igneous Province (∼ 90–76 Ma; APIP; Sgarbi and Valença, 1993; Melluso et al., 2008; Velásquez Ruiz et al., 2022) and Goiás Alkaline Province (∼ 90–80 Ma; GAP; Brod et al., 2005) in south-eastern Brazil (Fig. 1c), where abundant kamafugites occur that are associated with carbonatites, kimberlites and other alkaline rocks (e.g. lamprophyres; e.g. Guarino et al., 2013) in the Mata da Corda Formation.

This study presents the results of an experimental petrology investigation into four natural kamafugites from Toro Ankole (TA; sample 47), Alto Paranaíba Igneous Province (APIP; sample S.R.) and central Italy (San Venanzo – sample SAV6 – and Cupaello – sample CUL5). The latter two samples belong to the same volcanic province but are characterized by distinct petrographic, geochemical and isotopic compositions (e.g. Lustrino et al., 2020; Innocenzi, 2024). Experiments were performed on samples from each of the kamafugite type localities to allow a better characterization of the whole rock group and variations in the group's sources.

All four samples are mafic to ultramafic, ultrabasic and potassic to ultrapotassic in composition, which makes the identification of primitive samples particularly challenging.

Table 1. Whole-rock chemical data (wt %) for the starting material chosen for the experimental runs.

	TA	APIP	IAP	
Sample	47[a]	S.R.[b]	SAV6[c]	CUL5[d]
SiO_2	39.88	40.51	41.10	43.60
TiO_2	4.49	3.69	0.69	1.09
Al_2O_3	7.86	6.43	10.01	6.59
Fe_2O_{3tot}	12.17	12.75	7.05	7.06
MnO	0.21	0.21	0.12	0.11
MgO	9.40	14.72	12.89	9.94
CaO	14.15	10.34	15.74	15.86
Na_2O	1.50	2.74	0.97	0.38
K_2O	3.99	1.26	7.52	7.57
P_2O_5	1.21	1.27	0.38	1.18
LOI	4.83	4.99	1.46	4.34
CO_2	0.27		0.88	0.10
Total	99.69	93.92	98.81	97.83
Mg#	0.63	0.72	0.80	0.76

[a] Innocenzi et al. (2023). [b] Melluso et al. (2008). [c] Lustrino et al. (2020). [d] Lustrino et al. (2022a). LOI: mass loss on ignition. Mg# denotes Mg / ($Mg+Fe^{2+}$) assuming $Fe^{3+}/\Sigma Fe = 0.15$.

For instance, the Mg# values [Mg / ($Mg+Fe^{2+}$)] in primitive magmas of such compositions can be as low as 0.60 (Lloyd et al., 1985; Foley, 1992b), much lower than typical melts in equilibrium with peridotitic mantle sources. The lowest Mg# (calculated assuming $Fe^{3+}/\Sigma Fe = 0.15$) among the selected samples (0.63 in lava sample 47 from TA) could indicate primitive compositions in equilibrium with rocks richer in iron than the classical four-phase volatile-free peridotitic matrix (e.g. phlogopite-rich and olivine-poor veins). The Mg# of the Mg-richest starting composition is 0.80 (SAV6; Table 1), a value that, instead, could indicate olivine accumulation. TA and APIP samples share similar silica content but are characterized by different CaO, K_2O and Na_2O contents.

Natural samples were preferred in place of synthetic compositions to avoid results from an over-simplified system which does not match with natural mantle components. According to the International Union of Geological Sciences (IUGS) classification scheme (Le Maitre, 2002), the selected kamafugites (Table 1) are mafurite (olivine–pyroxene kalsilitite; sample 47, from TA), ugandite (pyroxene–olivine–kalsilite leucitite; sample Santa Rosa from APIP), venanzite (kalsilite–phlogopite–olivine–leucite melilitite; sample SAV6 from San Venanzo; IAP) and coppaelite (kalsilite–phlogopite melilitite; sample CUL5 from Cupaello; IAP). According to the IUGS definition, coppaelite has no olivine, but small amounts of this mineral occur in the investigated sample from Cupaello (Innocenzi, 2024). The natural starting materials were not doped with any additional elements, H_2O or CO_2.

2.1 Experimental details

Experiments were performed in a 0.5 in. rapid-quenching piston cylinder apparatus (Ezad et al., 2023) at the School of Natural Sciences, Macquarie University, Australia, using natural CaF_2 as the pressure medium. Temperatures were measured with $Pt_{30}Rh_{70}$–Pt_6Rh_{94} (B-type) thermocouples. An MDX-540 Roland mill was used to manufacture graphite capsules, hosting one to three holes, where samples can be loaded separately, allowing three compositions to be run simultaneously under the same pressure and temperature (P–T) conditions. Starting mixtures were loaded into the graphite capsules closed by a 0.5 mm thick graphite lid and subsequently wrapped in 25 µm thick Pt foil.

Pressure calibrations were based on the "albite = jadeite + quartz" reaction (Holland, 1980). All experiments were first brought to the desired pressure (1–2 GPa) before being rapidly heated to supra-liquidus conditions (1450 °C for Italian and Ugandan rocks and 1500 °C for Brazilian lavas) and then held for 1 h to ensure total melting of the starting materials. The experimental charges were then slowly cooled at a rate of 15 °C h^{-1} to near-liquidus temperature (1250–1380 °C, 15 experiments) or lower (1000–1150 °C, 3 experiments) and then held for 8 h. Two experiments (A22-118 and M22-087) were conducted with a short cooling time (3 h; ∼ 33 °C h^{-1}) and then were replicated (A22-125 and M22-103) cooling the charges for a longer time (8 and 11 h). The experiments were then quenched by cutting off power to the graphite furnace, reaching room temperature in ∼ 10 s.

2.2 Analytical methods

Samples were recovered and cut longitudinally by a diamond saw into two halves and then embedded in epoxy resin and polished to a 1 µm diamond finish. Quantitative chemical analyses and chemical mapping of the main mineral phases and glass were carried out on the experimental samples at Macquarie GeoAnalytical laboratories (Macquarie University) by quantitative energy-dispersive X-ray spectroscopy (quant-EDS) using a Zeiss EVO MA 15 scanning electron microscope (SEM), operating at 20 kV with a working distance of 12 mm and a beam current of 10 µA. The SEM is equipped with an Oxford Ultim Max 100 EDS detector. The data quality of this system has previously been documented by cross-checking its performance against results from a JEOL HAX 8530F wavelength-dispersive X-ray spectroscopy (WDS) electron microprobe at the University of Tasmania, with which data agree within a 2 % error (Shu et al., 2024). High-resolution images of the samples were acquired with an FEI Teneo FE SEM (field emission scanning electron microscope), equipped with two Bruker XFlash 6-30 EDS detectors and operating at 15 kV with an 11 nA beam current, a spot size ranging between 1 and 2 nm, and a working distance of 10 mm.

Table 2. Summary table for all the experiments carried out at different pressures and temperatures. The run products represent equilibrium phase assemblages (quench crystals are not mentioned). Abbreviations: ap, apatite; cpx, clinopyroxene; kal, kalsilite; ol, olivine; phl, phlogopite; ti, titanite.

Experiment	Pressure	Near-liquidus temperature	Run products
TA (Toro Ankole, Uganda)			
M22-086	2 GPa	1380 °C	melt
M22-083	2 GPa	1350 °C	melt, cpx, phl
A22-118	2 GPa	1330 °C	melt
A22-125	2 GPa	1330 °C	melt, cpx, phl, ap
M22-103	2 GPa	1330 °C	melt, cpx, phl, ap
A22-128	2 GPa	1290 °C	melt, cpx, phl, ap
A22-136	2 GPa	1000 °C	melt, cpx, phl, ap, ti
A23-004	1 GPa	1400 °C	melt
A23-002	1 GPa	1350 °C	melt
A23-003	1 GPa	1330 °C	melt
A23-005	1 GPa	1250 °C	melt, cpx
CUP (Cupaello – IAP, Italy)			
M22-086	2 GPa	1380 °C	melt
M22-083	2 GPa	1350 °C	melt, cpx, phl
A22-118	2 GPa	1330 °C	melt
A22-125	2 GPa	1330 °C	melt, cpx, phl, ap
A22-128	2 GPa	1290 °C	melt, cpx, phl, ap
A22-136	2 GPa	1000 °C	melt, cpx, phl, ap
A23-004	1 GPa	1400 °C	melt
A23-002	1 GPa	1350 °C	melt
A23-003	1 GPa	1330 °C	melt
A23-005	1 GPa	1250 °C	melt, cpx
SAV (San Venanzo – IAP, Italy)			
A23-006	2 GPa	1330 °C	melt, cpx, ol
A23-010	2 GPa	1250 °C	melt, cpx, ol, kal
A23-024	2 GPa	1150 °C	melt, cpx, ol, kal, phl
APIP (Alto Paranaíba Igneous Province, Brazil)			
M22-087	2 GPa	1380 °C	melt
M22-093	2 GPa	1350 °C	melt, cpx, ol
M22-103	2 GPa	1330 °C	melt, cpx, ol
A22-137	2 GPa	1000 °C	melt, cpx, ol, ap, oxides

3 Results

All results (Tables 2 to 7 and Tables S1 and S2 in the Supplement), classification diagrams (Figs. S1, S2 and S5 in the Supplement), images (Figs. S3 and S6) and chemical mapping (Fig. S4) of the samples are reported in the Supplement. Phenocrysts and microphenocrysts have been interpreted as equilibrium phases (Table 2), while small microliths found in the quenched melt have been interpreted as part of the glass. Their small size did not allow correct chemical characterization, leaving chemical mapping as the only tool to identify them.

3.1 Toro Ankole (Uganda)

Eleven experiments were conducted on the TA sample (Table 2). Average mineral and glass compositions are reported in Tables 3–7. Seven experiments were run at 2 GPa. At 1350 °C and 2 GPa, recovered TA glasses are very heterogeneous and mostly formed by quenched crystals, resulting in extreme compositions (e.g. SiO_2 ranging from 21.08 wt % to 25.88 wt %). With decreasing temperatures TA glass is mostly ultrabasic (SiO_2 37.18 wt %–45.96 wt %), with high TiO_2 (1.50 wt %–5.02 wt %) and CaO (10.51 wt %–15.27 wt %). K_2O content ranges between 1.18 wt % (1330 °C) and 7.34 wt % (1100 °C).

Table 3. Average chemical composition (SEM–EDS analyses, wt %) of the main mineral phases crystallizing in all the experiments on the TA sample (Uganda). All data are in Tables S1 and S2. The standard deviation value for each average composition is reported in italics.

Run	Conditions	SiO_2	TiO_2	Al_2O_3	FeO	MnO	MgO	CaO	K_2O	Na_2O	P_2O_5	BaO	SrO	Total	Number of analyses
Phlogopite															
M22-083	1350 °C (2 GPa)	38.95	2.53	14.47	6.76	–	21.58	–	10.74	–	–	0.74	–	95.77	3
σ		*0.79*	*0.22*	*0.34*	*0.36*	–	*0.33*	–	*0.10*	–	–	*0.15*	–		
A22-136	1000 °C (2 GPa)	35.68	6.47	14.16	13.12	0.08	14.14	–	10.00	0.17	–	0.30	–	94.12	3
σ		*0.28*	*0.08*	*0.29*	*0.56*	*0.13*	*0.55*	–	*0.26*	*0.15*	–	*0.53*	–		
Clinopyroxene															
M22-083	1350 °C (2 GPa)	50.34	1.69	5.00	4.49	–	14.45	22.97	0.19	0.62	–	–	–	99.73	4
σ		*1.99*	*0.62*	*1.22*	*1.34*	–	*1.44*	*1.10*	*0.37*	*0.12*	–	–	–		
A22-125	1330 °C (2 GPa)	44.54	5.71	7.41	8.09	–	11.00	19.95	0.75	1.02	1.06	–	–	99.65	8
σ		*1.07*	*0.21*	*0.59*	*0.65*	–	*0.99*	*1.40*	*0.63*	*0.17*	*0.11*	–	–		
A22-128	1290 °C (2 GPa)	51.48	1.35	3.67	4.28	0.04	15.03	22.76	–	0.46	–	–	–	99.07	5
σ		*0.41*	*0.22*	*0.44*	*0.16*	*0.06*	*0.16*	*0.28*	–	*0.05*	–	–	–		
A22-136	1000 °C (2 GPa)	49.82	1.35	4.19	8.57	0.23	11.96	22.40	–	0.71	–	–	–	99.21	4
σ		*0.87*	*0.25*	*0.28*	*4.92*	*0.11*	*3.50*	*0.23*	–	*0.26*	–	–	–		
A22-005	1250 °C (1 GPa)	51.62	1.96	3.01	2.40	–	16.88	24.21	–	0.08	–	–	–	100.15	5
σ		*1.41*	*0.39*	*0.46*	*0.19*	–	*0.74*	*0.83*	–	*0.12*	–	–	–		
Ti-magnetite															
M22-083	1350 °C (2 GPa)	9.57	18.16	1.70	47.57	1.16	2.75	5.12	1.07	1.57	–	–	–	88.67	1
Apatite															
A22-136	1100 °C (2 GPa)	2.30	–	–	0.84	–	0.31	51.23	0.38	–	41.01	–	1.21	94.98	4
σ		*0.69*	–	–	*0.13*	–	*0.16*	*0.82*	*0.20*	–	*1.63*	–			
Titanite															
M22-083	1350 °C (2 GPa)	30.26	23.57	3.81	5.04	–	2.18	27.13	–	0.07	1.40	–	–	93.39	3
σ		*0.65*	*1.66*	*0.90*	*0.77*	–	*0.41*	*0.53*	–	*0.13*	*0.44*	–	–		
A22-136	1000 °C (2 GPa)	28.93	35.96	2.13	1.02	–	0.05	27.03	–	–	–	–	–	95.11	3
σ		*0.49*	*0.68*	*0.22*	*0.15*	–	*0.08*	*0.16*	–	–	–	–	–		

The presence of phlogopite and clinopyroxene (Fig. 2), found as either large phenocrysts or small microphenocrysts, characterizes all the experiments. At 1350 °C, clinopyroxene with diopside composition (Fig. 3a) is less abundant than phlogopite (Fig. 4a). Phlogopite is Ti-rich (TiO_2 2.59 wt %–6.55 wt %) and is characterized by FeO_{tot} up to 13.76 wt % (Fig. 3c). Additional phases, occurring as microliths in the quenched glasses, are Ti-rich oxides and Ti-magnetite (Table 3; Figs. 5a and S4). This assemblage is later joined by apatite (1330 °C) and titanite (1000 °C; Tables 3, S1).

Four experiments were carried out at lower pressure (1 GPa). The runs between 1330 and 1400 °C returned glass only (Table S2), highlighting a steep liquidus line. At temperatures of 1250 °C, elongated diopside phenocrysts, with little CaO excess ($Wo_{45.3–51.0}En_{45.6–49.3}Fs_{1.00–5.4}$), are the only primary phase (Fig. 2).

3.2 Cupaello (IAP, Italy)

Seven CUP experiments were run at 2 GPa and three at 1 GPa (Table 2). The recovered glass at 1350 °C and 2 GPa (Table 7) has strongly ultrabasic and CaO-rich compositions, likely related to the heterogeneous and poorly quenched nature of glasses. Decreasing the temperature (from 1330 to 1290 °C

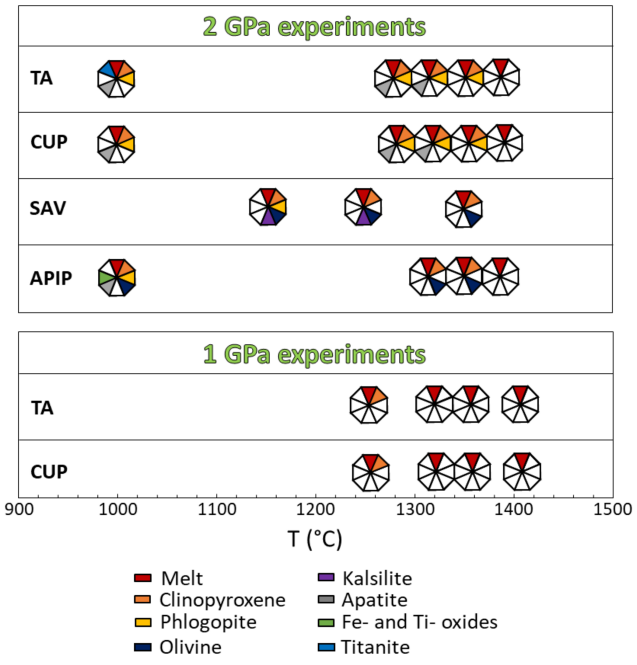

Figure 2. Appearance of phases in the experiments at 1 and 2 GPa.

and 2 GPa), CUP glass is ultrabasic (SiO_2 39.83 wt %–42.16 wt %) and enriched in CaO (6.26 wt %–14.02 wt %; Table S1 and Fig. S1), K_2O (7.71 wt %–12.46 wt %) and P_2O_5 (1.48 wt %–1.97 wt %).

All 2 GPa experiments at temperatures of 1350 °C and below show phlogopite and clinopyroxene crystallized as both large phenocrysts and small microphenocrysts (Fig. 2). Apatite appears at 1330 °C (Figs. 4b and 5b). Phlogopite is the dominant phase only at 1350 °C and is characterized by much lower TiO_2 (0.45 wt %–4.42 wt %) and FeO_{tot} (1.24 wt %–11.61 wt %) compared to TA phlogopite (Fig. 3c). BaO reaches up to 1.11 wt % (Tables 4 and S1). Clinopyroxenes are classified as diopside (Fig. 3a).

Experiments at 1 GPa show results comparable to those obtained for TA in the same experimental conditions: between 1330 and 1400 °C the system is a supra-liquidus system (Table S2), and diopside ($Wo_{48.7–49.5}En_{47.1–49.2}Fs_{1.3–3.0}$) is observed at 1250 °C (Fig. 2).

3.3 San Venanzo (IAP, Italy)

Three experiments were carried out on the SAV sample (Table 2) at 2 GPa. SAV glasses have low SiO_2 (35.43 wt %–39.36 wt %), coupled with high CaO (13.50 wt %–15.47 wt %) and K_2O (10.02 wt %–12.33 wt %). The ubiquitous near-liquidus phases for SAV experiments are subhedral Fo-rich ($Fo_{86.4–92.5}Fa_{6.2–12.4}La_{0.1–0.2}Tp_{0.0–1.2}$; Fig. 3b) olivine (Fig. 5c) and MgO-rich clinopyroxene with some CaO excess ($Wo_{50.9–54.9}En_{41.6–45.1}Fs_{0.3–6.1}$; Figs. 2 and 3a and Table S1). At 1250 °C, sub-rounded kalsilite is present (Table 5; Fig. 4c), whilst phlogopite appears in the lowest-temperature experiment (1150 °C; Fig. 2). Phlogopite shows high Al_2O_3 and MgO contents but low TiO_2 and FeO_{tot}.

3.4 Alto Paranaíba Igneous Province sample (Brazil)

Five experiments (Table 2) were run on the Brazilian sample at 2 GPa. The highest-temperature experiment (1380 °C) is above the liquidus, but quenched phases consisting of small clinopyroxene, phlogopite, apatite and oxides (Fe- and Ti-rich; Fig. 2) are observed in the glass. The glass compositions range from ultrabasic to basic (SiO_2 41.23 wt %–45.85 wt %) and show high TiO_2 (2.50 wt %–4.63 wt %) and MgO (12.70 wt %–16.34 wt %). Na_2O is higher than K_2O (see Tables 7 and S1). High-Mg olivine is the first and predominant near-liquidus phase ($Fo_{71.53–91.96}Fa_{7.55–27.82}La_{0.00–0.45}Tp_{0.20–0.41}$; Fig. 3b), followed by clinopyroxene needles (augite; Fig. 3a), Fe- and Ti-bearing oxides, and apatite in the quenched melt (Fig. 5d; Table 6). At 1000 °C, phlogopite, ilmenite (TiO_2 50.7 wt %–54.0 wt %, FeO_{tot} 32.8 wt %–34.9 wt %; Table 6) and apatite are present (Fig. 3).

4 Discussion

The liquidus minerals produced in these experiments represent the main mineral phases in equilibrium with kamafugitic melts in given P–T conditions. According to the "inverse approach" used in experimental petrology (e.g. Wyllie, 1987), they can be considered the main contributors to the chemistry of the kamafugitic melts of Uganda, Brazil and Italy investigated. Petrographic studies of the natural samples helped us to select compositions without xenocrysts, xenoliths or cumulates, and whole-rock geochemical data do not outline fractionation trends among the studied rocks. These features justify the assertion that their chemistry should not differ substantially from real magma compositions (see Sect. 2).

Orthopyroxene has never been found as a liquidus phase in the experiments for any of the samples investigated, and, consequently, it is unlikely to be a common constituent of the mantle sources of the Toro Ankole, Alto Paranaíba and Intra-Apennine provinces. Melt compositions with low SiO_2 and high K_2O can, however, be explained by melting of phlogopite and clinopyroxene (Funk and Luth, 2013; Foley and Ezad, 2024; Shu et al., 2024). Modal variations in these two phases, coupled with the differing abundances of accessory minerals, including titanite and ilmenite, may account for the geochemical variability in magmas among the three volcanic provinces. To highlight these differences, each kamafugite is considered separately in the following sections.

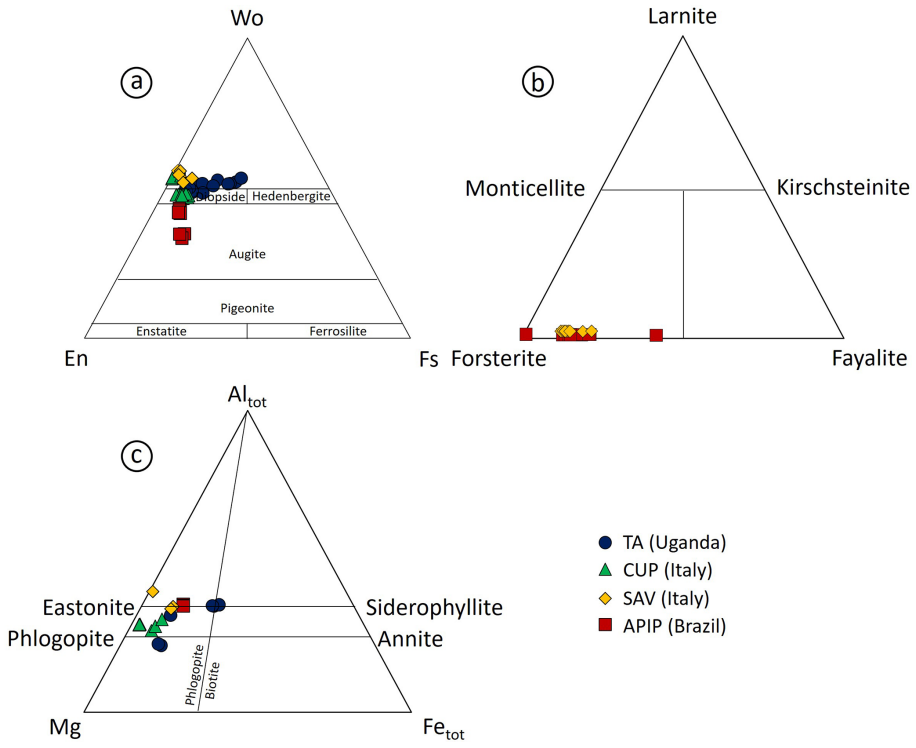

Figure 3. **(a)** Wollastonite–enstatite–ferrosilite diagram (after Morimoto, 1988) for experimental clinopyroxene compositions from TA, CUP, SAV and APIP samples. **(b)** Forsterite–fayalite–larnite diagram for experimental olivine compositions from TA, CUP, SAV and APIP samples. **(c)** Al_{tot}–Mg–Fe_{tot} diagram for experimental phlogopite compositions from TA, CUP, SAV and APIP samples.

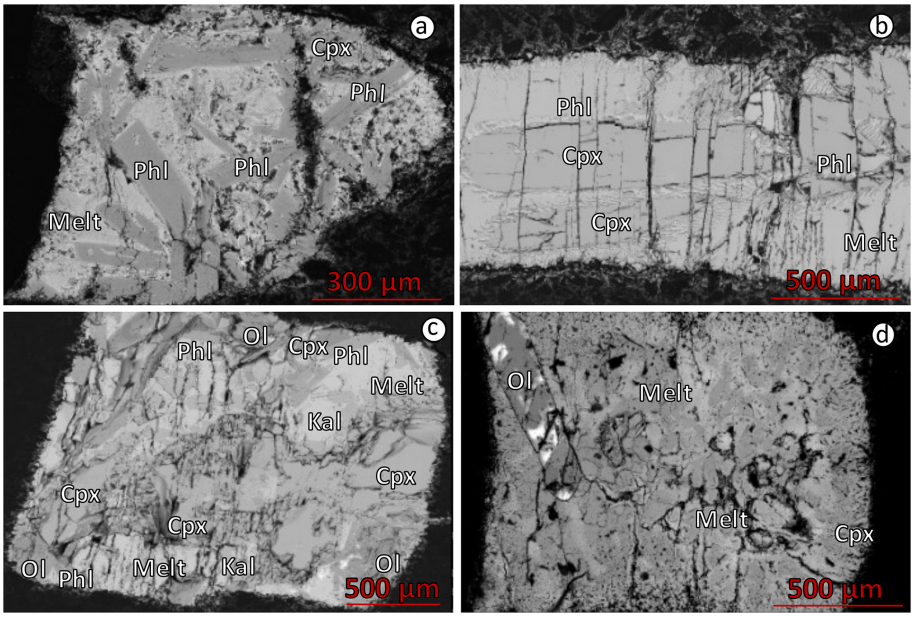

Figure 4. FE SEM micrographs of experimental samples. **(a)** Euhedral phenocrysts of phlogopite and microphenocrysts of clinopyroxene from the TA sample (M22-083 experiment, 1350 °C and 2 GPa). **(b)** Phlogopite around clinopyroxene phenocrysts in the CUP sample (A22-125 experiment, 1330 °C and 2 GPa). **(c)** Anhedral clinopyroxene phenocrysts coupled with euhedral phlogopite, olivine and kalsilite in the SAV sample (A23-024 experiment, 1150 °C and 2 GPa). **(d)** Euhedral olivine phenocryst and clinopyroxene microphenocrysts from the APIP sample (M22-093 experiment, 1350 °C and 2 GPa). Abbreviations as in Table 2.

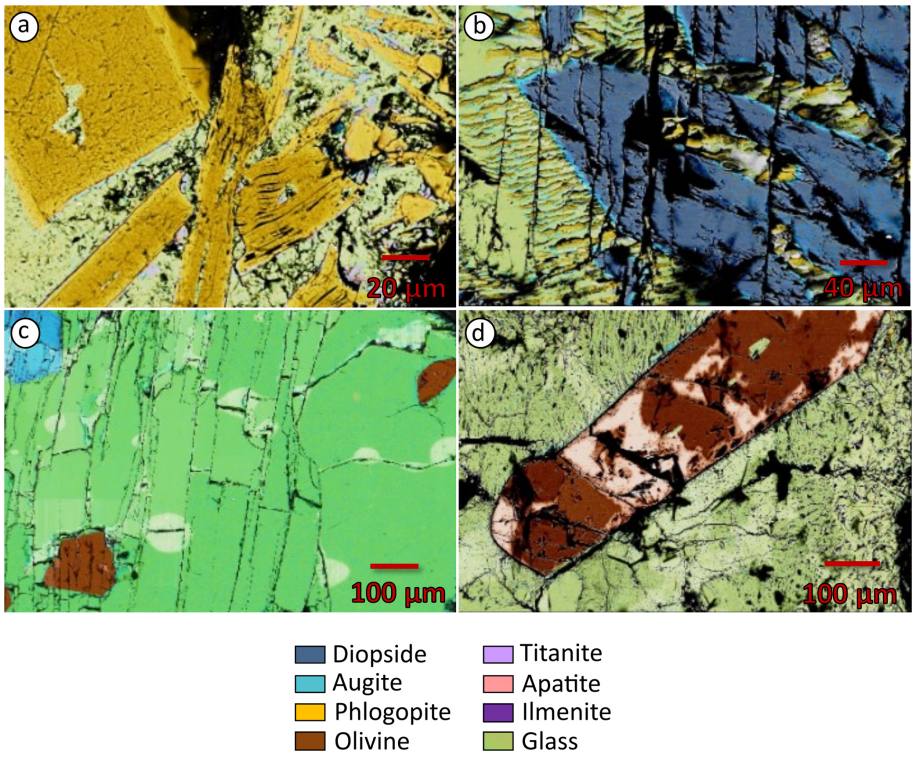

Figure 5. FE SEM compositional maps of experimental samples. **(a)** TA sample M22-083 (1350 °C and 2 GPa). **(b)** CUP sample A22-125 (1330 °C and 2 GPa). **(c)** SAV sample A23-006 (1330 °C and 2 GPa). **(d)** APIP sample M22-093 (1350 °C and 2 GPa).

Table 4. Averaged chemical composition (SEM–EDS analyses, wt %) of the main mineral phases crystallizing in all the experiments on the CUP sample (Italy). All data are in Tables S1 and S2. The standard deviation value for each average composition is reported in italics.

Experiment	Conditions	SiO_2	TiO_2	Al_2O_3	FeO	MnO	MgO	CaO	K_2O	P_2O_5	BaO	Total	Number of analyses
Phlogopite													
M22-083	1350 °C (2 GPa)	40.68	0.42	13.77	1.33	–	26.53	–	11.1	–	0.99	94.79	3
σ		*0.32*	*0.03*	*0.05*	*0.15*	–	*0.25*		*0.07*	–	*0.10*		
A22-125	1330 °C (2 GPa)	41.99	2.32	12.32	4.69	0.04	22.54		10.65	–	0.23	94.79	3
σ		*0.29*	*0.25*	*1.03*	*0.53*	*0.08*	*0.51*	–	*0.15*	–	*0.40*		
A22-136	1000 °C (2 GPa)	37.51	4.33	14.33	11.00	0.05	17.11	–	10.13	–	0.69	95.15	3
σ		*0.16*	*0.10*	*0.24*	*0.53*	*0.09*	*0.60*	–	*0.45*	–	*0.60*		
Clinopyroxene													
M22-083	1350 °C (2 GPa)	51.07	0.68	4.69	1.29	–	16.33	25.40	–	–	–	99.45	4
σ		*0.65*	*0.34*	*0.71*	*0.57*	–	*0.69*	*0.05*	–	–	–		
A22-125	1330 °C (2 GPa)	55.09	0.17	1.61	1.75	–	17.90	24.07	–	–	–	100.68	4
σ		*0.42*	*0.22*	*0.43*	*0.14*	–	*0.35*	*0.37*	–	–	–		
A22-128	1290 °C (2 GPa)	53.91	0.31	1.76	2.56	–	16.88	23.70	–	–	–	99.11	4
σ		*0.51*	*0.26*	*0.67*	*0.17*	–	*0.21*	*0.39*	–	–	–		
A22-136	1000 °C (2 GPa)	54.84	0.32	–	2.28	–	17.36	24.19	–	–	–	99.00	4
σ		*0.56*	*0.03*	–	*0.16*	–	*0.44*	*0.13*	–	–	–		
A22-005	1250 °C (1 GPa)	53.79	0.38	1.09	2.24	–	17.52	24.73	–	–	–	99.73	2
σ		*0.35*	*0.05*	*0.05*	*0.04*	–	*0.01*	*0.08*	–	–	–		
Apatite													
A22-136	1000 °C (2 GPa)	1.28	1.58	–	–	–	0.32	51.85	0.15	42.71	–	97.89	3
σ		*0.22*	*0.07*	–	–	–	*0.03*	*0.47*	*0.13*	*0.60*	–		

Table 5. Average chemical composition (SEM–EDS analyses, wt %) of the main mineral phases crystallizing in all the experiments on the SAV sample (Italy). All data are in Tables S1 and S2. The standard deviation value for each average composition is reported in italics.

Experiment	Conditions	SiO_2	TiO_2	Al_2O_3	FeO	MnO	MgO	CaO	K_2O	Na_2O	P_2O_5	BaO	Total	Number of analyses
Phlogopite														
A23-024	1100 °C (2 GPa)	38.73	1.48	16.57	6.41	0.20	22.22	–	10.77	–	–	0.38	96.76	3
σ		*0.48*	*0.12*	*0.58*	*0.27*	*0.34*	*0.59*	–	*0.26*	–	–	*0.04*		
Clinopyroxene														
A23-010	1250 °C (2 GPa)	49.12	0.56	7.08	2.40	–	14.31	24.74	0.04	0.08	–	–	98.33	3
σ		*0.36*	*0.14*	*0.16*	*0.10*	–	*0.39*	*0.41*	*0.07*	*0.14*	–	–		
A23-024	1100 °C (2 GPa)	50.49	0.40	6.61	1.99	0.04	15.21	25.12	–	–	–	–	100.09	3
σ		*0.41*	*0.07*	*0.47*	*0.24*	*0.06*	*0.30*	*0.96*	–	–	–	–		
Olivine														
A23-006	1330 °C (2 GPa)	40.92	–	–	6.27	0.13	52.10	0.88	–	–	–	–	100.30	3
σ		*1.13*	–	–	*0.05*	*0.01*	*1.60*	*0.02*	–	–	–	–		
A23-010	1250 °C (2 GPa)	40.04	–	–	9.30	0.11	48.96	0.91	–	–	–	–	99.31	4
σ		*0.66*	–	–	*2.22*	*0.12*	*1.98*	*0.04*	–	–	–	–		
A23-024	1100 °C (2 GPa)	40.69	–	–	7.23	0.12	51.07	0.87	–	–	–	–	99.98	4
σ		*0.38*	–	–	*0.46*	*0.03*	*0.64*	*0.02*	–	–	–	–		
Kalsilite														
A23-010	1250 °C (2 GPa)	37.45	–	31.33	0.41	–	–	–	29.84	0.46	–	–	99.49	3
σ		*0.46*	–	*0.59*	*0.09*	–	–	–	*0.15*	*0.08*	–	–		
A23-024	1100 °C (2 GPa)	37.75	–	31.83	0.36	–	–	–	29.33	0.58	–	–	99.84	3
σ		*0.75*	–	*0.64*	*.0.4*	–	–	–	*0.70*	*0.05*	–	–		

Table 6. Average chemical composition (SEM–EDS analyses, wt %) of the main mineral phases crystallizing in all the experiments on the APIP sample (Brazil). All data are in Tables S1 and S2. The standard deviation value for each average composition is reported in italics.

Experiment	Conditions	SiO_2	TiO_2	Al_2O_3	FeO	MnO	MgO	CaO	K_2O	Na_2O	P_2O_5	BaO	Cr_2O_3	Total	Number of analyses
Phlogopite															
A22-137	1000 °C (2 GPa)	36.46	6.04	15.02	7.61	–	18.23	–	8.43	0.91	–	2.38	–	95.07	3
σ		*0.18*	*0.11*	*0.28*	*0.05*	–	*0.11*	–	*0.12*	*0.08*	–	*0.22*	–		
Clinopyroxene															
M22-093	1350 °C (2 GPa)	48.71	3.75	6.70	6.92	–	16.28	13.98	0.06	1.73	0.52	–	0.20	98.86	3
σ		*0.81*	*0.18*	*0.37*	*0.21*	–	*0.28*	*0.44*	*0.10*	*0.29*	*0.05*	–	*0.04*		
A22-137	1000 °C (2 GPa)	53.06	1.06	2.73	3.94	0.08	17.30	19.62	–	0.84	–	–	–	98.61	4
σ		*0.10*	*0.23*	*0.48*	*0.15*	*0.09*	*0.10*	*0.37*	–	*0.10*	–	–	–		
Olivine															
M22-093	1350 °C (2 GPa)	40.48	–	–	9.47	0.11	49.20	0.29	–	–	–	–	–	99.54	8
σ		*0.72*	–	–	*2.08*	*0.07*	*1.67*	*0.01*	–	–	–	–	–		
M22-103	1330 °C (2 GPa)	39.92	–	–	7.36	0.14	50.29	0.26	–	–	–	–	–	97.97	1
A22-137	1000 °C (2 GPa)	40.00	–	–	14.28	0.24	45.13	0.23	–	–	–	–	–	99.88	4
σ		*1.75*	–	–	*7.52*	*0.11*	*5.61*	*0.06*	–	–	–	–	–		
Ilmenite															
A22-137	1000 °C (2 GPa)	0.03	54.08	0.38	34.91	0.47	7.27	0.07	–	–	–	–	–	97.21	3
σ		*0.06*	*0.21*	*0.02*	*1.83*	*0.05*	*0.23*	*0.12*	–	–	–	–	–		
Apatite															
A22-137	1000 °C (2 GPa)	0.23	–	–	0.81	–	0.37	51.58	–	0.54	43.62	0.51	0.32	97.97	3
σ		*0.40*	–	–	*0.04*	–	*0.35*	*1.63*	–	*0.22*	*2.40*	–	–		

Table 7. Average chemical composition (SEM–EDS analyses, wt %) of the glasses resulting from all the experiments. All data are in Tables S1 and S2. The standard deviation value for each average composition is reported in italics.

Experiment	Conditions	SiO_2	TiO_2	Al_2O_3	FeO	MnO	MgO	CaO	K_2O	Na_2O	P_2O_5	SO_3	ZrO_2	BaO	SrO	Total	Number of analyses
TA (Toro Ankole, Uganda)																	
M22-083	1350 °C (2 GPa)	24.55	6.15	3.12	10.18	0.36	3.61	32.07	2.36	2.51	4.30	–	–	–	1.66	90.85	4
σ		*2.32*	*1.11*	*1.14*	*1.42*	*0.04*	*1.24*	*5.01*	*0.79*	*0.11*	*2.68*	–	–	–	*0.16*		
A22-128	1290 °C (2 GPa)	39.38	4.90	8.38	11.33	0.22	9.11	14.07	4.71	1.52	1.37	–	–	0.80	0.96	96.73	4
σ		*0.77*	*0.14*	*0.17*	*0.12*	*0.02*	*0.19*	*0.22*	*0.11*	*0.05*	*0.08*	–	–	*0.92*	*0.58*		
M22-103	1330 °C (2 GPa)	41.05	4.31	9.17	7.57	0.13	10.90	14.87	2.07	3.10	1.10	–	–	0.14	–	94.39	6
σ		*1.04*	*0.13*	*0.44*	*0.58*	*0.07*	*0.52*	*0.35*	*0.13*	*0.89*	*0.16*	–	–	*0.22*	–		
A22-136	1100 °C (2 GPa)	41.04	1.85	10.69	8.10	0.38	0.61	11.57	7.01	2.91	1.10	–	–	0.46	1.55	87.25	4
σ		*3.70*	*0.26*	*1.35*	*1.39*	*0.04*	*0.17*	*1.22*	*0.38*	*0.56*	*0.18*	–	–	*0.04*	*0.11*		
CUP (Cupaello – IAP, Italy)																	
M22-083	1350 °C (2 GPa)	23.59	1.56	2.11	4.62	0.09	10.42	35.63	4.20	0.96	2.34	0.44	0.64	–	1.54	88.12	4
σ		*0.54*	*0.07*	*0.13*	*0.28*	*0.10*	*0.47*	*0.34*	*0.16*	*0.04*	*0.19*	*0.37*	*0.02*	–	*0.05*		
A22-125	1330 °C (2 GPa)	40.61	1.55	7.91	4.61	0.06	12.05	13.86	7.90	0.90	1.53	0.13	–	0.20	0.91	92.20	4
σ		*0.65*	*0.07*	*0.10*	*0.04*	*0.07*	*0.16*	*0.15*	*0.11*	*0.04*	*0.06*	*0.15*	–	*0.28*	*0.61*		
A22-128	1290 °C (2 GPa)	41.21	1.35	8.24	6.64	0.04	10.40	12.79	7.90	0.85	1.90	0.29	–	1.24	0.64	93.45	4
σ		*0.27*	*0.04*	*0.09*	*0.12*	*0.08*	*0.17*	*0.05*	*0.23*	*0.06*	*0.06*	*0.03*	–	*0.83*	*0.05*		
A22-136	1100 °C (2 GPa)	43.94	2.07	10.03	4.86	0.15	4.83	4.95	15.10	1.06	–	0.09	–	0.79	–	87.85	3
σ		*1.00*	*0.10*	*0.13*	*0.64*	*0.01*	*0.09*	*0.22*	*0.21*	*0.09*	–	*0.20*	–	*0.25*	–		
SAV (San Venanzo – IAP, Italy)																	
A23-006	1330 °C (2 GPa)	39.34	0.86	11.32	5.15	–	10.10	15.37	10.08	1.15	0.38	–	–	–	–	93.76	3
σ		*0.02*	*0.05*	*0.16*	*0.07*	–	*0.19*	*0.13*	*0.05*	*0.03*	*0.05*	–	–	–	–		
A23-010	1250 °C (2 GPa)	35.53	1.11	9.82	8.44	–	6.99	13.77	11.13	1.79	0.75	–	–	–	–	89.33	3
σ		*0.13*	*0.06*	*0.03*	*0.08*	–	*0.49*	*0.43*	*0.43*	*0.15*	*0.13*	–	–	–	–		
A23-024	1150 °C (2 GPa)	32.87	1.17	8.14	10.82	0.26	6.47	16.41	11.79	2.65	1.43	–	–	–	–	92.00	5
σ		*0.81*	*0.04*	*0.21*	*0.27*	*0.01*	*0.14*	*0.29*	*0.34*	*0.11*	*0.11*	–	–	–	–		
APIP (Alto Paranaíba Igneous Province, Brazil)																	
M22-093	1350 °C (2 GPa)	42.61	4.19	6.71	10.38	–	13.91	11.27	1.20	2.70	1.01	0.03	0.18	–	0.31	94.51	7
σ		*1.42*	*0.21*	*0.18*	*0.85*	–	*1.24*	*0.88*	*0.06*	*0.43*	*0.23*	*0.09*	*0.03*	–	*0.23*		
M22-103	1330 °C (2 GPa)	45.29	4.47	7.87	5.77	0.11	16.15	14.51	0.55	1.42	0.74	–	–	–	–	96.88	3
σ		*0.76*	*0.18*	*0.36*	*0.83*	*0.10*	*0.26*	*1.19*	*0.70*	*0.32*	*0.09*	–	–	–	–		
A22-137	1100 °C (2 GPa)	42.49	3.14	9.59	9.10	0.15	15.28	9.05	0.94	3.62	–	–	–	–	–	93.37	3
σ		*0.71*	*0.56*	*1.62*	*0.05*	*0.06*	*0.41*	*0.54*	*0.08*	*0.03*	–	–	–	–	–		

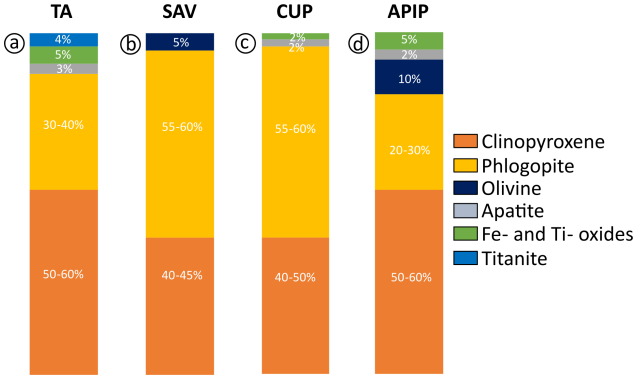

Figure 6. Estimates of mineral phase abundances involved in the melting reactions of the kamafugite rocks investigated. **(a)** Toro Ankole Province. **(b)** San Venanzo (IAP). **(c)** Cupaello (IAP). **(d)** Alto Paranaíba Igneous Province.

4.1 Experimental implications for mantle source paragenesis

4.1.1 Toro Ankole (Uganda)

Diopside and Ti-rich phlogopite are ubiquitous minerals in the TA experiments, with clinopyroxene often being the most abundant liquidus phase (Fig. 4a). Accessory phases recorded by the experiments are titanite (Figs. S3–S4), apatite and Fe–Ti-rich oxides (ilmenite and magnetite s.s.) identified by chemical mapping (Fig. S4). No Fe–Ti oxides were found in the 1000 °C experiment, probably due to both the large amount of titanite crystallization and the high TiO_2 content of phlogopite. Clinopyroxene and phlogopite are considered to be the main phases contributing to TA melts, with a 50 %–60 % and 30 %–40 % modal abundance, respectively (Fig. 6a), followed by ∼ 3 % apatite, ∼ 2 %–4 % titanite and ∼ 3 %–5 % Ti-magnetite (Fig. 6a). Such minor phases are typically associated with metasomatized mantle (e.g.MARID – mica–amphibole–rutile–ilmenite–diopside; Fitzpayne et al., 2018) and would play a key role in determining the contents of minor constituents and trace elements in TA melts (Foley and Ezad, 2024).

4.1.2 Intra-Apennine Province (Italy)

Diopside is also the liquidus phase in the IAP experiments. It is present in all lower-temperature runs and, in many cases, as the predominant mineral phase (Fig. 4b–c). The other near-liquidus phase in the Cupaello experiments is phlogopite, but phlogopite crystallizes in the SAV runs only at much lower temperatures. This is probably due to kalsilite crystallization in the higher-K_2O (7.52 wt %) SAV experiments at 1250 and 1150 °C. However, kalsilite is unlikely to be a source constituent: although its stability can extend to depths greater than 100 km (Wendlandt and Eggler, 1980a), it can only exist in near-anhydrous conditions because even minimum amounts of water can allow stabilization of phlogopite (Wendlandt and Eggler, 1980b). The presence of kalsilite in the current experiments is related to the low H_2O content of the starting material, considering that the SAV6 sample has only ∼ 3 % modal phlogopite associated with olivine phenocrysts (Lustrino et al., 2020). Water was not added to the starting compositions, so the low H_2O content prevented phlogopite formation, resulting in kalsilite accommodating the excess K_2O budget. IAP phlogopite has TiO_2 contents that vary between 0.39 wt % (1350 °C) and 4.42 wt % (1000 °C), accommodating all the TiO_2 in the 1000 and 1150 °C experiments as no Fe–Ti oxides are present.

San Venanzo is characterized by the presence of olivine as an additional liquidus mineral, a phase not observed in Cupaello, probably due to its lower MgO content (∼ 10 wt % in Cupaello vs. ∼ 13 wt % in San Venanzo). Based on mineral chemical and isotopic compositions, Günther et al. (2023) suggested that some of the olivines in San Venanzo kamafugites are phenocrysts, while others are xenocrysts sampled from a lamproite magma batch during their ascent. Without going into detail about lamproitic vs. kamafugitic composition of San Venanzo primary magma, we underline the fact that the interpretation of Günther et al. (2023) could explain the larger amount of olivine in SAV runs compared to the other kamafugite samples. On this basis, we estimate that only 5 % of olivine participates during the partial melting process in the San Venanzo mantle source.

Cupaello results indicate proportions of ∼ 55 %–60 % modal phlogopite and ∼ 40 %–50 % clinopyroxene in the melting assemblage (Fig. 6b), overlapping the results obtained for San Venanzo (∼ 55 %–60 % modal phlogopite and ∼ 40 %–45 % clinopyroxene; Fig. 6c). The IAP mantle therefore has the highest phlogopite content among the districts investigated, explaining the highest K_2O in the magmatic products. Considering that the IAP rocks are characterized by the most radiogenic Sr isotopic ratios by far (Lustrino et al., 2020; Innocenzi, 2024), the phlogopite in their sources could be related to ancient metasomatic processes and is not necessarily related to any coeval subduction beneath Italy (e.g. Lustrino et al., 2022a).

Accessory minerals are absent in SAV experiments, while apatite crystallized in the CUP sample. This reflects the different whole-rock geochemical compositions of the Italian kamafugites, considering that one of their most distinctive features is the lower TiO_2 and P_2O_5 (0.73 wt %–1.11 wt % and 0.23 wt %–1.64 wt %) compared to the contents of TA ($TiO_2 = 3.55$ wt %–5.79 wt % and $P_2O_5 = 0.09$ wt %–1.57 wt %) and APIP samples ($TiO_2 = 3.61$ wt %–6.38 wt % and $P_2O_5 = 0.30$ wt %–4.21 wt %; see Innocenzi, 2024, and references therein). This would imply only minimal amounts, if any, of magnetite and apatite (in both cases < 2 %) joining the partial melting in CUP mantle (Fig. 6b).

4.1.3 Differences between the two Italian samples

The experiment results based on the Italian samples (San Venanzo and Cupaello) deserve further discussion. The starting materials are from two kamafugite outcrops, part of the same volcanic province, 70 km apart. Nevertheless, they exhibit many different features in terms of petrography (San Venanzo lavas have high modal olivine content, whereas in Cupaello, olivine is only a rare groundmass phase), major element oxides (San Venanzo lavas have not only slightly higher MgO and Al_2O_3 but also much lower P_2O_5) and trace elements (Cupaello lavas have higher LILE, HFSE, LREE and Pb–Th–U contents; Lustrino et al., 2020; Innocenzi, 2024). Lustrino et al. (2022b) explained these compositional variations invoking a kalsilite + melilite + olivine fractionation, starting from an olivine–leucite–kalsilite melilitite (a composition similar to that of San Venanzo kamafugite) and generating a derivative melt corresponding to the Cupaello lava.

In order to explore other possible interpretations, we conducted near-liquidus experiments on both compositions. Experimental results from this study highlight that both melts are in equilibrium with phlogopite and clinopyroxene, which are required to produce the basic and ultrapotassic compositions found in San Venanzo and Cupaello.

Both hypotheses (slightly different mantle sources vs. fractional crystallization) can be valid and are supported by petrographic and geochemical clues. Further experimental studies (e.g. partial melting experiments) must be carried out to fully resolve this issue. The small volume of magma emplaced at Cupaello and its exotic chemical composition could be explained by melt extraction exclusively tapping metasomatic veins. On the other hand, the reactive nature of the melt would probably have led to interactions with surrounding peridotite wall rock, resulting in a compositional modification and dilution of the exotic characteristics of a kamafugite magma in the San Venanzo case.

4.1.4 Alto Paranaíba Igneous Province (Brazil)

Past studies of APIP samples (e.g. Brod et al., 2005; Melluso et al., 2008; Guarino et al., 2013; Velásquez Ruiz et al., 2022) have highlighted their altered nature (e.g. partial replacement of leucite by analcime resulting in LOI values of up to 6 %; Innocenzi, 2024, and reference therein). This may account for the relatively low K_2O and higher Na_2O content in APIP samples, a common characteristic in other ultrapotassic compositions such as lamproites (e.g. Prelević et al., 2004). However, even accounting for the action of alteration processes, the low alkali content shown by the APIP kamafugites seems, at least partially, to be a primary feature. After all, great attention was paid to selecting the samples for the experiments among the least altered APIP products.

The main feature of the experiments on the APIP sample is the occurrence of olivine as a liquidus phase (Fig. 5d), likely due to higher MgO contents in the APIP starting composition ($\sim$ 15 wt %) compared to IAP samples (10 wt %–13 wt %) and TA (9 wt %). APIP samples are, in general, also characterized by the lowest K_2O within the kamafugite rock group. Small needles of clinopyroxene are found in all the liquidus experiments performed on the APIP sample, with CaO-poorer (13.70 wt %–19.98 wt %) and Na_2O-richer (up to 2.05 wt %) compositions (augite; Fig. 3a) compared to TA and IAP clinopyroxene. Nevertheless, the Na_2O content of augite tends to decrease with temperature from 1350 to 1000 °C, probably due to the increasing amount of clinopyroxene. The APIP source is probably enriched in clinopyroxene, and its composition must differ from the typical mantle diopside, to explain Na_2O contents of melts of up to 4 wt % (Innocenzi, 2024). Prelević et al. (2004) suggested that, due to secondary analcime crystallization, almost all the current Na_2O content in some lamproitic rocks was initially K_2O. This is not true for kamafugite samples (Prelević et al., 2004), which contain K-rich nepheline and Na-bearing kalsilite, as recorded in APIP lavas (e.g. Melluso et al., 2008; Innocenzi, 2024). Therefore, we assume that most of the Na_2O is primary and that K_2O was originally only slightly higher.

In the APIP experiments, TiO_2-rich phlogopite crystallized only at 1000 °C (Fig. 5c). We relate the late appearance of phlogopite to the low K_2O of the starting material (1.26 wt %), reflecting the generally low K_2O enrichment of the APIP magmas (Innocenzi, 2024). Lower modal phlogopite in the APIP source is consistent with the lower K_2O / Na_2O ratio of the magmatic products, which ranges from 1.4 to 7.2. Different accessory phases (Fe–Ti oxides, mainly ilmenite s.s. and apatite) are recorded in the experiments with the APIP sample (Table S1 and Fig. S4). Summing up, we estimate that for APIP magmas, the mineral phases contributing to the melt comprise up to $\sim$ 50 %–60 % clinopyroxene, $\sim$ 20 %–30 % phlogopite, $\sim$ 10 % olivine, $\sim$ 3 %–5 % ilmenite and $\sim$ 2 % apatite (Fig. 6d).

4.2 Further constraints on kamafugite mantle sources

Experiments on the four selected kamafugites compositions show quite similar results. A ubiquitous component in the mantle sources of kamafugite magmas is clinopyroxene. Clinopyroxene-rich sources ensure the high CaO content of melts and suppress the Na_2O content. As an alternative hypothesis, the high CaO content (and the overall ultracalcic compositions, i.e. $CaO/Al_2O_3 > 1$) may be related to the presence of carbonates in the kamafugite mantle sources. However, considering the low CO_2 content of the natural samples (likely due to CO_2 degassing at shallow depths before magma solidification), the CaO component attributed to mantle carbonate would be hidden in the clinopyroxene component. In support of this hypothesis, Brazilian and Ugandan kamafugites are associated with carbonatites (Melluso et al., 2008; Innocenzi et al., 2024a), while in the Italian cases, the calcite-rich compositions are related to assimilation of sedimentary carbonates (e.g. Lustrino et al., 2019, 2020, 2022b).

The appearance of olivine in the APIP and SAV runs and the conclusion that olivine may be present in their sources could indicate the effect of the infiltration of the partial melts into the peridotitic matrix and their reaction with it. Clinopyroxene–phlogopite-rich metasomatic veins have much lower solidus temperatures compared with their surrounding peridotite (e.g. Lloyd et al., 1985; Foley et al., 2022; Ezad et al., 2024; Shu et al., 2024). Therefore, partial melting most likely starts in these phlogopite-bearing clinopyroxenite networks, with anatexis that may proceed to involve the adjacent peridotite matrix, with which metasomatic melts may interact and react during their upwelling (Foley, 1992a). By reacting with a peridotite mantle, FeO-rich melts can increase their MgO content, reducing their mobility and probably crystallizing at depth as a consequence of the higher solidus of MgO-rich compositions (Foley et al., 1999). As these melts are probably not mobile enough to reach the Earth surface, another hypothesis is that peridotite interacts with K-rich fluids during earlier metasomatic events. Variable degrees of interaction among the neighbouring depleted mantle and the phlogopite–clinopyroxene-rich assemblages are required to explain not only the geochemical differences recorded among TA, APIP and IAP, but also the great variability observed among the various eruptive centres of the same province.

Experimental results point out the key role of accessory phases in the genesis of Ugandan (apatite + titanite + Ti-magnetite) and Brazilian kamafugites (apatite + ilmenite). The presence of accessory phases in the source explains not only the major oxide compositions (e.g. the extremely high TiO_2 contents recorded in TA and APIP samples), but also the high contents of incompatible trace elements recorded in the natural compositions (e.g. Melluso et al., 2008; Innocenzi et al., 2024a; Foley and Ezad, 2024), considering that apatite and titanite are usually strongly enriched in Sr, HFSE and LREE (Tiepolo et al., 2002; Prowatke and Klemme,

2006). The crystallization of such minerals may also explain the HREE / LREE fractionation recorded in the natural kamafugite lavas (e.g. Pitcavage et al., 2021; Innocenzi et al., 2024a). Further evidence that supports their involvement in kamafugite petrogenesis comes from the ultramafic nodules, including those found in TA and APIP lavas and in many other alkaline rocks (such as MARID or PIC – phlogopite–ilmenite–clinopyroxene – xenoliths; e.g. Fitzpayne et al., 2018).

The need for a phlogopite- and clinopyroxene-rich mantle has been demonstrated by previous studies on natural compositions (e.g. Foley, 1992a; Lustrino et al., 2020; Guarino et al., 2024; Innocenzi et al., 2024a, 2024b). Indeed, mineralogical features such as the presence of rare phases in kamafugite groundmass (kalsilite and minor calcite), major oxide (ultrabasic to basic and K_2O-rich), trace element (strong LILE enrichment) and isotopic (radiogenic Sr and Pb ratios and unradiogenic Nd) data have been interpreted as being derived from a strongly metasomatized lithospheric mantle, in which veins, enriched in carbonate, phlogopite and clinopyroxene, create a complex network in the peridotite matrix (Guarino et al., 2013; Lustrino et al., 2020; Pitcavage et al., 2021; Innocenzi et al., 2024a).

This hypothesis is further supported by the mineralogy of nodules carried to the surface by the potassic and ultrapotassic lavas (e.g. Guarino et al., 2024). Even if their exact origin (e.g. kamafugite source or cumulates from strongly alkaline magmas) is still controversial, their presence testifies to the unusual mineralogical makeup of the underlying mantle. The modal composition of TA nodules matches the paragenesis of the melting assemblage reconstructed in this study well, as these nodules are mainly composed of phlogopite and diopside, as well as accessory phases including magnetite, titanite, apatite and perovskite. In accordance with our results, those nodules are devoid of olivine and orthopyroxene (e.g. Link et al., 2008). On the other hand, APIP nodules range from lherzolite to metasomatized peridotite and glimmerite (e.g. Gaspar et al., 2003). The less metasomatized nature of these nodules is consistent with the low phlogopite content and the high modal abundance of olivine in the experimental results from this study.

As for the Toro Ankole Province, Edgar et al. (1976) and Arima and Edgar (1982) conducted near-liquidus experiments at 1–3 GPa on each of the archetypical kamafugite types (mafurite, katungite, ugandite) from the western branch of the East African Rift, with the variable addition of H_2O and CO_2. In their studies, olivine appears as the first near-liquidus phase, followed by clinopyroxene, phlogopite and ilmenite. The main difference with the results reported here is the lack of olivine as a liquidus phase in the TA sample, which is probably related to the different starting material compositions. The TA sample used in this study has much lower MgO content (9 wt %) compared to the compositions of Edgar et al. (1976; 14 wt %–20 wt % MgO). This could reflect a strong heterogeneity found not only in the natural samples, but also in the mantle sources, where different relative abundances of each mineral might be found, along with slightly different degrees of partial melting or with slightly different degrees of interaction with the peridotite matrix.

On the other hand, it is important to highlight that the high MgO contents of the compositions investigated by Edgar et al. (1976) may not represent primary melt compositions but are probably the consequence of abundant olivine antecrysts in the samples (e.g. Holmes, 1942). Lloyd et al. (1985) reported partial melting experiments at 1175–1300 °C and 2–3 GPa on a phlogopite-bearing clinopyroxenite (as well as Ti-magnetite, titanite and apatite), with similar conclusions to those in this study. They found that melt composition at a degree of partial melting of 20 %–30 % closely resembles Toro Ankole kamafugite lavas.

5 Conclusions

This study attempts to constrain the mantle source compositions of kamafugites from the three worldwide type localities by means of near-liquidus experiments. Experimental results support the hypothesis that the mantle sources underlying the three volcanic provinces (TA, APIP and IAP) share similar paragenesis, with phlogopite and clinopyroxene as the main silicate constituents; this is clearly different from the classical mantle peridotite (olivine + clinopyroxene + orthopyroxene ± spinel/garnet).

The geochemical and isotopic heterogeneities recorded by kamafugites from the various localities are reflected in the experimental results, which also suggest that variable amounts of phlogopite and clinopyroxene are involved in the melting reactions of the three sources. The TA and APIP melting assemblages are probably phlogopite-bearing (∼ 30 %–40 % in TA and ∼ 20 %–30 % in APIP) clinopyroxenites, whereas the IAP melting assemblages are clinopyroxene-bearing (∼ 40 %–50 %) glimmerite. The presence of olivine as a liquidus phase distinguishes APIP (∼ 10 %) and SAV (∼ 5 %) samples, in agreement with the high-MgO rock compositions and the lower K_2O content of the APIP rocks.

Several accessory phases are found in the experimental samples, with variable abundances in the different provinces. SAV experiments recorded no accessory phases. In other runs, apatite is quite common, together with Ti–Fe oxides. The Ugandan kamafugite is probably characterized by the highest contribution of accessory phases to the melt (e.g. ∼ 3 % apatite, ∼ 2 %–4 % titanite and ∼ 3 %–5 % Ti-magnetite); this is similar to the mineralogy of ultramafic nodules carried by the lavas. APIP probably requires only ∼ 2 % apatite and ∼ 3 %–5 % ilmenite or Ti-magnetite.

Orthopyroxene is absent in the mantle sources of the kamafugitic magmas investigated. Carbonates may be present at the source but did not occur in the experiments because the compositions investigated in the experiments had undergone

CO_2 degassing from the primary magmas at shallow depths. This CaO excess explains the extremely calcic composition of clinopyroxenes and an overall ultracalcic composition of natural kamafugites.

Data availability. All the data we collected in this study can be found in the Excel file submitted as the Supplement.

Supplement. The supplement related to this article is available online at: https://doi.org/10.5194/ejm-36-899-2024-supplement.

Author contributions. FI: investigation, visualization, data curation, writing (original draft). ISE: investigation, conceptualization, writing (review and editing). SR: writing (review and editing). SA: resources, writing (review and editing). ML: resources, writing (review and editing). SFF: conceptualization, resources, writing (review and editing).

Competing interests. The contact author has declared that none of the authors has any competing interests.

Disclaimer. Publisher's note: Copernicus Publications remains neutral with regard to jurisdictional claims made in the text, published maps, institutional affiliations, or any other geographical representation in this paper. While Copernicus Publications makes every effort to include appropriate place names, the final responsibility lies with the authors.

Special issue statement. This article is part of the special issue "Probing the Earth: experiments on and for our planet". It is a result of the EMPG 2023 conference, Milan, Italy, 12–15 June 2023.

Acknowledgements. The authors are grateful to Leone Melluso (University of Naples Federico II, Italy) for sharing the Brazilian kamafugite sample. The present work was financially supported by funds under IGG–CNR P-CT0049 awarded to Samuele Agostini; by ARC grant FL180100134 to Stephen F. Foley, Isra S. Eza and Francesca Innocenzi; and by Sapienza Ateneo 2021–2022–2023 grants to Michele Lustrino and Sara Ronca. Francesca Innocenzi is grateful to Slava Shcheka for his continuous help in the HP laboratories and to Sean Murray for his help in the Macquarie GeoAnalytical laboratories. Francesca Innocenzi also thanks Lorenzo Fedele (University of Naples Federico II, Italy) and Michele Mattioli (University of Urbino Carlo Bo, Italy) for their help in improving the readability of the paper. The paper strongly benefitted from the detailed comments and suggestions of the two anonymous reviewers and Dejan Prelević (University of Belgrade, Serbia).

Financial support. This research has been supported by the Istituto di Geoscienze e Georisorse, Consiglio Nazionale delle Ricerche (grant no. P-CT0049), Australian Research Council (grant no. FL180100134) and Sapienza Ateneo 2021–2022–2023 grants.

Review statement. This paper was edited by Francois Holtz and reviewed by Dejan Prelević and two anonymous referees.

References

Anderson, D. L.: Speculations on the nature and cause of mantle heterogeneity, Tectonophysics, 416, 7–22, https://doi.org/10.1016/j.tecto.2005.07.011, 2006.

Arima, M. and Edgar, A. D.: High pressure experimental studies on a katungite and their bearing on the genesis of some potassium-rich magmas of the west branch of the African rift, J. Petrol., 24, 166–187, https://doi.org/10.1093/petrology/24.2.166, 1982.

Brod, J. A., Barbosa, E. S. R., Junqueira-Brod, T. C., Gaspar, J. C., Diniz-Pinto, H. S., Sgarbi, P. B. A., and Petrinovic, I. A.: The Late-Cretaceous Goiás Alkaline Province (GAP), Central Brazil, In Mesozoic to Cenozoic Alkaline Magmatism in the Brazilian Platform, edited by: Comin-Chiaramonti, P. and Gomes, C. B., Edusp/Fapesp, São Paulo, 261–340, 2005.

Carvalho, J. B. and Leonardos, O. H.: Preliminary geothermobarometric and metasomatism studies on mantle xenoliths of kimberlites and associated rocks from the Alto Paranaiba, SE Brazil, Int. Kimberlite Conf. Ext. Abstr., 6, 101–103, 1995.

Edgar, A. D., Green, D. H., and Hibberson, W. O.: Experimental petrology of a highly potassic magma, J. Petrol., 17, 339–356, https://doi.org/10.1093/petrology/17.3.339, 1976.

Ezad, I. S., Shcheka, S. S., Buhre, S., Buhre, A., Gorojovsky, L. R., Shea, J. J., Förster, M. W., and Foley, S. F.: Rapid quench piston cylinder apparatus: An improved design for the recovery of volatile-rich geological glasses from experiments at 0.5–2.5 GPa, Rev. Sci. Instrum., 94, https://doi.org/10.1063/5.0129417, 2023.

Ezad, I. S., Blanks, D. E., Foley, S. F., Holwell, D. A., Bennett, J., and Fiorentini, M. L.: Lithospheric hydrous pyroxenites control localisation and Ni endowment of magmatic sulfide deposits, Miner. Deposita, 59, 227–236, https://doi.org/10.1007/s00126-023-01238-z, 2024.

Fitzpayne, A., Giuliani, A., Phillips, D., Hergt, J., Woodhead, J. D., Farquhar, J., Fiorentini, M. L., Drysdale, R. N., and Wu, N.: Kimberlite-related metasomatism recorded in MARID and PIC mantle xenoliths, Miner. Petrol., 112, 71–84, https://doi.org/10.1016/j.lithos.2018.08.036, 2018.

Foley, S. F.: Vein-plus-wall-rock melting mechanisms in the lithosphere and the origin of potassic alkaline magmas, Lithos, 28, 435–453, https://doi.org/10.1016/0024-4937(92)90018-T, 1992a.

Foley, S. F.: Petrological characterization of the source components of potassic magmas: geochemical and experimental constraints, Lithos, 28, 187–204, https://doi.org/10.1016/0024-4937(92)90006-K, 1992b.

Foley, S. F. and Ezad, I. S.: Melting of hydrous pyroxenites with alkali amphiboles in the continental mantle: 2. Trace element compositions of melts and minerals, Geosci. Front., 15, 101692, https://doi.org/10.1016/j.gsf.2023.101692, 2024.

Foley, S. F. and Pintér, Z: Primary melt compositions in the Earth's mantle, in: Magmas Under Pressure, edited by: Kono,

Y. and Sanloup, C., Elsevier, Amsterdam, Netherlands, 3–42, https://doi.org/10.1016/B978-0-12-811301-1.00001-0, 2018.

Foley, S. F., Venturelli, G., Green, D. H., and Toscani, L.: The ultrapotassic rocks: characteristics, classification, and constraints for petrogenetic models, Earth-Sci. Rev., 24, 81–134, https://doi.org/10.1016/0012-8252(87)90001-8, 1987.

Foley, S. F., Musselwhite, D. S., and van der Laan, S. R.: Melt compositions from ultramafic vein assemblages in the lithospheric mantle: a comparison of cratonic and non-cratonic settings, in: Proceedings of Cape Town Kimberlite Conference, Red Roof Publishers, Cape Town, J.B. Dawson vol., 238–246, ISBN 0799218642, 9780799218640, 1999.

Foley, S. F., Andronikov, A. V., and Melzer, S.: Petrology of ultramafic lamprophyres from the Beaver Lake area of Eastern Antarctica and their relation to the breakup of Gondwanaland, Mineral. Petrol., 74, 361–384, https://doi.org/10.1007/s007100200011, 2002.

Foley, S. F., Ezad, I. S., van der Laan, S. R., and Petermann, M.: Melting of hydrous pyroxenites with alkali amphiboles in the continental mantle: 1. Melting relations and major element composition of melts, Geosci. Front., 13, 101380, https://doi.org/10.1016/j.gsf.2022.101380, 2022.

Förster, M. W., Prelević, D., Buhre, S., Mertz-Kraus, R., and Foley, S. F.: An experimental study of the role of partial melts of sediments versus mantle melts in the sources of potassic magmatism, J. Asian Earth Sci., 177, 76–88, https://doi.org/10.1016/j.jseaes.2019.03.014, 2019.

Funk, S. P. and Luth, R. W.: Melting phase relations of a mica–clinopyroxenite from the Milk River area, southern Alberta, Canada, Contrib. Mineral. Petrol., 166, 393–409, https://doi.org/10.1007/s00410-013-0881-6, 2013.

Gallo, F., Giammetti, F., Venturelli, G., and Vernia, L.: The kamafugitic rocks of S. Venanzo and Cupaello, Central Italy, Neues Jb. Miner. Monat., 5, 198–210, 1984.

Gaspar, J. C., Araújo, A. L. N., Carlson, R. W., Sichel, S. E., Brod, J. A, Sgarbi, P. B., and Danni, J. C. M.: Mantle xenoliths and new constraints on the origin of alkaline ultrapotassic rocks from the Alto Paranaíba and Goiás igneous provinces, Brazil, International Kimberlite Conference: Extended Abstracts, Victoria, Canada, June 2003, 8, 1–5, 2003.

Guarino, V., Wu, F. Y., Lustrino, M., Melluso, L., Brotzu, P., de Barros Gomes, C., Ruberti, E., Tassinari, C. C. G., and Svisero, D. P.: U–Pb ages, Sr–Nd-isotope geochemistry, and petrogenesis of kimberlites, kamafugites and phlogopite-picrites of the Alto Paranaíba Igneous Province, Brazil. Chem. Geol., 353, 65–82, https://doi.org/10.1016/j.chemgeo.2012.06.016, 2013.

Guarino, V., Bonazzi, M., Nimis, P., Azzone, R. G., Cariddi, B., and Zanetti, A.: Stabilization and evolution of the Brazilian subcontinental lithospheric mantle: insights from garnet xenocrysts and peridotite xenoliths of Três Ranchos kimberlite (APIP, Brazil), Gondwana Res., 130, 18–35, https://doi.org/10.1016/j.gr.2024.01.005, 2024.

Gülmez, F., Prelević, D., Forster, M. W., Buhre, S., and Günther, J.: Experimental production of K-rich metasomes through sediment recycling at the slab mantle interface in the fore-arc, Sci. Rep., 13, 19608, https://doi.org/10.1038/s41598-023-46367-7, 2023.

Günther, J., Prelević, D., Mertz, D. F., Rocholl, A., Mertz-Kraus, R., and Conticelli, S.: Subduction-Legacy and Olivine Monitoring for Mantle-Heterogeneities of the Sources of Ultrapotassic Magmas: The Italian Case Study, Geochem. Geophy. Geosy., 24, e2022GC010709, https://doi.org/10.1029/2022GC010709, 2023.

Holland, T. J.: The reaction albite= jadeite+ quartz determined experimentally in the range 600–1200 C, Am. Mineral., 65, 129–134, 1980.

Holmes, A.: A suite of volcanic rocks from south-west Uganda containing kalsilite (a polymorph of $KAlSiO_4$), Mineral. Mag., 26, 197–217, 1942.

Holmes, A.: Petrogenesis of katungite and its associates, Am. Mineral., 35, 772–792, 1950.

Holmes, A.: The potash ankaratrite-mela-leucitites lavas from Nabugando and Mbuga craters, South/West Uganda, Trans. R. Soc. Edinb., 15, 187–213, 1952.

Innocenzi, F.: Origin of "ultra" rocks, Unpublished PhD thesis, Sapienza University of Rome, 538 pp., 2024.

Innocenzi, F., Ronca, S., Foley, S. F., Agostini, S., and Lustrino, M.: Exotic magmatism from the western branch of the East African Rift: insights on the lithospheric mantle source., EGU General Assembly 2022, Vienna, Austria, 23–27 May 2022, EGU22-5450, https://doi.org/10.5194/egusphere-egu22-5450, 2022.

Innocenzi, F., Agostini, S., Foley, S. F., Ronca, S., and Lustrino, M.: Kamafugites and kamafugites: a comparison of the Ugandan, Brazilian and Italian variants, Goldschmidt 2023 Conference, Lyon, France, 9–14 July 2023, https://doi.org/10.7185/gold2023.16259, 2023.

Innocenzi, F., Ronca, S., Foley, S. F., Agostini, S., and Lustrino, M.: Carbonatite and ultrabasic magmatism at Toro Ankole and Virunga, western branch of the East African Rift system, Gondwana Res., 125, 317–342, https://doi.org/10.1016/j.gr.2023.09.005, 2024a.

Innocenzi, F., Ronca, S., Agostini, S., Benedetti F., and Lustrino, M.: On the occurrence of kalsilite in melilite-bearing ultrapotassic lavas from the Roman Province (Vulsini Mts., central Italy), Lithos, 482–483, 107704, https://doi.org/10.1016/j.lithos.2024.107704, 2024b.

Le Maitre, R. W. (Ed.): Classification of Igneous Rocks and Glossary of Terms, Recommendations of the IUGS Subcommission on the systematics of igneous rocks, Cambridge University Press, New York, United States, 236 pp., ISBN-13 978-0-521-66215-4, 2002.

Link, K., Barifaijo, E., Tiberindwa, J., and Foley, S. F.: Veined pyroxenite xenoliths from the kamafugites in the Toro Ankole region of western Uganda: a window to a rift-related mantle, 9th Int. Kimberlite Conf. Ext. Abstr. 9IKC-A-00403, Frankfurt, Germany, October 2008, 1–3, 2008.

Link, K., Tommasini, S., Braschi, E., Conticelli, S., Barifaijo, E., Tiberindwa, J. V., and Foley, S. F.: Veined pyroxenite xenoliths in Ugandan kamafugites: mantle or magma? Using in situ techniques for $^{87}Sr/^{86}Sr$-isotopes and trace elements as tools, EGU General Assembly, Vienna, Austria, 2–7 May 2010, EGU2010-12701-1, 2010.

Lloyd, F. E.: Upper-mantle metasomatism beneath a continental rift: clinopyroxenes in alkaline mafic lavas and nodules from South-West Uganda, Mineral. Mag., 44, 315–323, https://doi.org/10.1180/minmag.1981.044.335.12, 1981.

Lloyd, F. E.: Experimental melting and crystallisation of glassy olivine melilitites, Contrib. Mineral. Petrol., 90, 236–243, https://doi.org/10.1007/BF00378264, 1985.

Lloyd, F. E., Arima, M., and Edgar, A. D.: Partial melting of a phlogopite-clinopyroxenite nodule from south-west Uganda: an experimental study bearing on the origin of highly potassic continental rift volcanics, Contrib. Mineral. Petrol., 91, 321–329, https://doi.org/10.1007/BF00374688, 1985.

Lustrino, M., Luciani, N., and Stagno, V.: Fuzzy petrology in the origin of carbonatitic/pseudocarbonatitic Ca-rich ultrabasic magma at Polino (central Italy), Sci. Rep., 9, 9212, https://doi.org/10.1038/s41598-019-45471-x, 2019.

Lustrino, M., Ronca, S., Caracausi, A., Ventura Bordenca, C., Agostini, S., and Faraone, D. B.: Strongly SiO_2-undersaturated, CaO-rich kamafugitic Pleistocene magmatism in Central Italy (San Venanzo volcanic complex) and the role of shallow depth limestone assimilation, Earth-Sci. Rev., 208, 103256, https://doi.org/10.1016/j.earscirev.2020.103256, 2020.

Lustrino, M., Pistocchi, L., Ronca, S., Innocenzi, F., and Agostini, S.: Carbonate assimilation of ultrabasic magma: The Pleistocene Cupaello kamafugitic volcano (central Italy), EGU General Assembly 2022, Vienna, Austria, 23–27 May 2022, EGU22-5673, https://doi.org/10.5194/egusphere-egu22-5673, 2022a.

Lustrino, M., Chiarabba, C., and Carminati, E.: Igneous activity in central-southern Italy: Is the subduction paradigm still valid?, in: In the Footsteps of Warren B. Hamilton: New ideas in Earth Science, edited by: Foulger, G. R., Hamilton, L. C., Jurdy, D. M., Stein, C. A., Howard, K. A., and Stein, S., Geol. Soc. Am. Spec. Paper, 553, 355–370, https://doi.org/10.1130/2021.2553(28), 2022b.

Melluso, L., Lustrino, M., Ruberti, E., Brotzu, P., De Barros Gomes, C., Morbidelli, L., Morra, V., Svisero, D. P., and d'Amelio, F.: Major and trace-element compositions of olivine, perovskite, clinopyroxene, Cr-Fe-Ti oxides, phlogopite and host kamafugites and kimberlites, Alto Paranaiba, Brazil, Can. Mineral., 46, 19–40, 10.3749/canmin.46.1.19, 2008.

Morimoto, N.: Nomenclature of pyroxenes, Am. Mineral., 73, 1123–1133, 1988.

Muravyeva, N. S. and Senin, V. G.: Xenoliths from Bunyaruguru volcanic field: some insights into lithology of East African Rift upper mantle, Lithos, 296, 17–36, https://doi.org/10.1016/j.lithos.2017.10.023, 2018.

Muravyeva, N. S., Belyatsky, B. V., Senis, V. G., and Ivanov, A. V.: Sr–Nd–Pb isotope systematics and clinopyroxene-host disequilibrium in ultra-potassic magmas from Toro Ankole and Virunga, East-African Rift: Implications for magma mixing and source heterogeneity, Lithos, 210–211, 260–277, https://doi.org/10.1016/j.lithos.2014.09.011, 2014.

Oliveira, I. L., Brod, J. A., Junquiera-Brod, T. C., Reimold, W. U., and Fuck, R. A.: The IUGS nomenclature on kalsilite-bearing volcanic rocks: a critical appraisal and recommendations, J. Petrol., 63, egac026, https://doi.org/10.1093/petrology/egac026, 2022.

Pertermann, M. and Hirschmann, M. M.: Anhydrous partial melting experiments on MORB-like eclogite: phase relations, phase compositions and mineral–melt partitioning of major elements at 2–3 GPa, J. Petrol., 44, 2173–2201, https://doi.org/10.1093/petrology/egg074, 2003.

Pintér, Z., Foley, S. F., Yaxley, G. M., Rosenthal, A., Rapp, R. P., Lanati, A. W., and Rushmer, T: Experimental investigation of the composition of incipient melts in upper mantle peridotites in the presence of CO_2 and H_2O, Lithos, 396, 106224, https://doi.org/10.1016/j.lithos.2021.106224, 2021.

Pitcavage, E., Furman, T., Nelson, W., Kalegga, P. K., and Barifaijo, E.: Petrogenesis of primitive lavas from the Toro Ankole and Virunga Volcanic Provinces: Metasomatic mineralogy beneath East Africa's Western Rift, Lithos, 106192, https://doi.org/10.1016/j.lithos.2021.106192, 2021.

Prelević, D., Foley, S. F., Cvetkovic, V., and Romer, R. L.: The analcime problem and its impact on the geochemistry of ultrapotassic rocks from Serbia, Mineral. Mag., 68, 621–638, https://doi.org/10.1180/0026461046840209, 2004.

Prelević, D., Jacob, D. E., and Foley, S. F.: Recycling plus: a new recipe for the formation of Alpine-Himalayan orogenic mantle lithosphere, Earth Planet. Sc. Let., 362, 187–197, https://doi.org/10.1016/j.epsl.2012.11.035, 2013.

Prowatke, S. and Klemme, S.: Trace element partitioning between apatite and silicate melts, Geochim. Cosmochim. Ac., 70, 4513–4527, https://doi.org/10.1016/j.gca.2006.06.162, 2006.

Rosenthal, A., Foley, S. F., Pearson, D. G., Nowell, G. M., and Tappe, S.: Petrogenesis of strongly alkaline primitive volcanic rocks at the propagating tip of the western branch of the East African Rift, Earth Planet. Sc. Let., 284, 236–248, https://doi.org/10.1016/j.epsl.2009.04.036, 2009.

Sgarbi, P. D. A. and Valença, J. G.: Kalsilite in Brazilian kamafugitic rocks, Mineral. Mag. 57, 165–171, https://doi.org/10.1180/minmag.1993.057.386.16, 1993.

Shu, C. T., Foley, S. F., Ezad, I. S., Daczko, N. R., and Shcheka, S. S.: Experimental melting of phlogopite websterite in the upper mantle between 1.5 and 4.5 GPa, J. Petrol., 65, egae030, https://doi.org/10.1093/petrology/egae030, 2024.

Stixrude, L. and Lithgow-Bertelloni, C.: Geophysics of chemical heterogeneity in the mantle, Annu. Rev. Earth Planet. Sci., 40, 569–595, https://doi.org/10.1146/annurev.earth.36.031207.124244, 2012.

Stoppa, F. and Cundari, A.: Origin and multiple crystallization of the kamafugite-carbonatite association: the San Venanzo-Pian di Celle occurrence (Umbria, Italy), Mineral. Mag., 62, 273–289, https://doi.org/10.1180/002646198547530, 1998.

Stracke, A.: A process-oriented approach to mantle geochemistry, Chem. Geol., 579, 120350, https://doi.org/10.1016/j.chemgeo.2021.120350, 2021.

Tappe, S., Foley, S. F., and Pearson, D. G.: The Kamafugites of Uganda: a mineralogical and geochemical comparison with their Italian and Brazilian analogues, Period. Mineral., 72, 51–77, 2003.

Tappe, S., Foley, S. F., Kjarsgaard, B. A., Romer, R. L., Heaman, L. M., Stracke, A., and Jenner, G. A.: Between carbonatite and lamproite – diamondiferous Torngat ultramafic lamprophyres formed by carbonate fusion melting of cratonic MARID-type metasomes, Geochim. Cosmochim. Ac., 72, 3258–3286, https://doi.org/10.1016/j.gca.2008.03.008, 2008.

Tiepolo, M., Oberti, R., and Vannucci, R.: Trace-element incorporation in titanite: constraints from experimentally determined solid/liquid partition coefficients, Chem. Geol. 191, 105–119, https://doi.org/10.1016/S0009-2541(02)00151-1, 2002.

Velásquez Ruiz, F., Cordeiro, P., Reich, M., Motta, J. G., Ribeiro, C. C., Angerer, T., and Bernardes, R. B.: The genetic link between kamafugite magmatism and alkaline–carbonatite complexes in the Late Cretaceous Alto Paranaíba

Igneous Province, Central Brazil, Int. Geol. Rev., 65, https://doi.org/10.1080/00206814.2022.2127127, 2022.

Wallace, M. E. and Green, D. H.: An experimental determination of primary magma composition, Nature, 335, 343–346, https://doi.org/10.1038/335343a0, 1988.

Wendlandt, R. F. and Eggler, D. H.: The origins of potassic magmas: 1. Melting relations in the systems $KAlSiO_4$-Mg_2SiO_4-SiO_2 and $KAlSiO_4$-MgO-SiO_2-CO_2 to 30 kilobars, Am. J. Sci., 280, 385–420, 1980a.

Wendlandt, R. F. and Eggler, D. H.: The origins of potassic magmas: 2. Stability of phlogopite in natural spinel lherzolite and in the system $KAlSiO_4$-MgO-SiO_2-H_2O-CO_2 at high pressures and high temperatures, Am. J. Sci., 280, 421–458, 1980b.

Wyllie, P. J.: Volcanic rocks: boundaries from experimental petrology, Fortschr. Mineral., 65, 249–284, 1987.